

# REP: Resource-Efficient Prompting for Rehearsal-Free Continual Learning

Sungho Jeon, Xinyue Ma, Kwang In Kim, Myeongjae Jeon  
POSTECH

{sunghojeon, xinyuema, kimkin, mj.jeon}@postech.ac.kr

## Abstract

*Recent rehearsal-free methods, guided by prompts, excel in vision-related continual learning (CL) with drifting data but lack resource efficiency, making real-world deployment challenging. In this paper, we introduce Resource-Efficient Prompting (REP), which improves the computational and memory efficiency of prompt-based rehearsal-free methods while minimizing accuracy trade-offs. Our approach employs swift prompt selection to refine input data using a carefully provisioned model and introduces adaptive token merging (AToM) and layer dropping (ALD) for efficient prompt updates. AToM and ALD selectively skip data and model layers while preserving task-specific features during new task learning. Extensive experiments on multiple image classification datasets demonstrate REP’s superior resource efficiency over state-of-the-art ViT- and CNN-based methods.*

## 1. Introduction

Continual learning (CL) trains neural network models on multiple sequential tasks, where each task may include data that diverges from previously encountered data. A crucial challenge for any CL algorithm is to effectively address *catastrophic forgetting* [24]. Severe forgetting occurs when a model rapidly loses previously learned knowledge while adapting to new tasks. The inability to adapt to new tasks not only impairs overall model accuracy but also affects user experiences of AI services in the real world [40].

Moreover, many of today’s AI services are designed for on-device scenarios [10, 20, 42] to securely learn tasks *locally*, without dependence on remote servers over the network. In on-device CL, learning methods must be optimized for *computational* (equivalently, *energy*) and *memory efficiency* requirements. Energy is scarce and can be intermittent in small devices in the wild [1, 15, 19], yet it is quickly drained by GPU operations during training [23]. Thus, achieving higher computational efficiency while training a new task in CL invariably enhances device durability. In contrast, memory efficiency often acts as a

hard constraint. Device memory capacity is typically very limited and unified to operate all CPU and GPU programs. Therefore, a CL task that exhausts all available memory risks system crashes due to out-of-memory errors. As mobile and edge devices adhere to small form factors, it is difficult to dramatically augment battery and memory capacity to address these issues in practice.

In this paper, we present several new techniques to reduce the computational and memory costs of *prompt-based rehearsal-free* methods that leverage frozen, pre-trained vision transformer (ViT) models [16, 31, 37–39]. Prompts are a small set of parameters that progressively learn incoming tasks to combat forgetting. Updates to these compact prompts incur *minimum data writes* without significantly harming the lifespan of device storage, which typically sustains up to 10K writes per location. This makes using prompts a good fit for on-device CL. Moreover, thanks to recent advancements in small-memory ViT models, such as ViT-Ti [32] (5.8M parameters; similar size to ResNet-10), we can always spot powerful ViT models that match the resource efficiency of traditional CNN models under consideration across memory specifications of typical resource-constrained IoT and embedded devices, as shown in Table 1.

To enhance prompt-based CL for resource efficiency, we introduce REP (Resource-Efficient Prompting; Figure 1). REP is built upon our analysis of cost-accuracy trade-offs across the end-to-end learning process, with two key design insights. (1) The *prompt selection* stage, which constructs a prompt subset to augment input or intermediate data, is highly amenable to numerous promising options with fast approximations. (2) In contrast, the *prompt update* stage, which involves forward-backward passes over the backbone model, presents a range of optimizations with vastly different cost-accuracy trade-offs. With these insights, we develop three complementary techniques for both stages that trade minimal accuracy drop for high resource efficiency: (1) *model downsizing* for prompt selection and (2) *adaptive token merging* (AToM) and *adaptive layer dropping* (ALD) for prompt update. In pre-trained ViT models, task-specific knowledge is concentrated in shallow layers, while generalized feature information is spread across all layers [38]

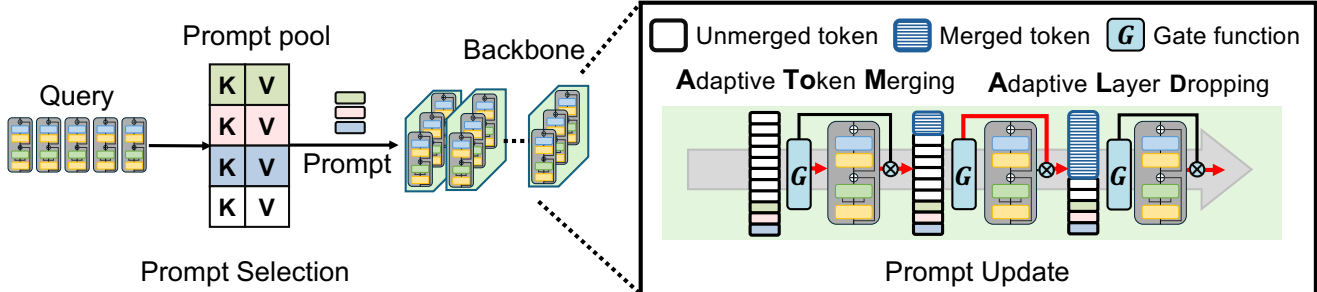


Figure 1. Overview of the proposed resource-efficient prompting (REP) algorithm for rehearsal-free CL. REP calculates query features from input samples using a lightweight model (e.g., ViT-Ti) to swiftly extract prompts from the prompt pool. These prompts are then inserted into a main backbone model (e.g., ViT-L) for training, which prioritizes model accuracy.

Table 1. ViT- and CNN-based methods with specific backbone models are mapped to the memory capacity they can fit into. DualP is DualPrompt, and CODA-P is CODA-Prompt.

Memory Capacity	ViT-Based Methods	CNN-Based Methods
4-8 GB	L2P (ViT-L), DualP (ViT-L) CODA-P (ViT-B)	MEMO (RN26, RN34) BudgetCL (RN101)
1-4 GB	L2P (ViT-B), DualP (ViT-B)	MEMO (RN10, RN18) BudgetCL (RN34)
Up to 1 GB	L2P (ViT-Ti), DualP (ViT-Ti)	BudgetCL (RN10, RN18)

(See Figure 2 for our analysis). So, AToM and ALD carry out selective skipping across the data and model-layer dimensions in a “non-uniform” manner to preserve critical task-specific features in the shallow layers. REP provides resource efficiency that aligns with the capabilities of real-world commodity devices including NVIDIA Jetson TX2 and Nano. We evaluate REP across various memory budgets, backbone models, and datasets. Our experiments demonstrate that REP reduces training iteration time by up to 52% and lowers memory consumption by up to 32%.

## 2. Related Work

**Class-Incremental Learning:** Our work primarily targets class-incremental learning (CIL) among various CL scenarios. In CIL, each incoming task introduces new classes within the same domain during the training phase, while task ID is not at hand during the inference phase [8]. In prior art using CNN backbone networks, *rehearsal-based* methods, which archive and replay representative samples from previous tasks [2, 4, 5, 30], have been a popular choice due to their superior performance [27]. Several recent methods are noteworthy along this line. For instance, BudgetCL [28] and CarM [21] suggest data-driven methods that outperform other strategies based on algorithmic optimizations, particularly when training is constrained by compute budgets. MEMO [43] effectively trades memory used to store

old samples for saving task-specific model layers. We compare prompt-based methods with some of these methods and confirm better performance under resource constraints.

**Continual Learning for the Edge:** There has been a notable emphasis on efficient memory and energy usage in on-device learning, particularly in non-CL settings [9, 35, 36]. More recently, a handful of studies have explored extending CL capabilities to edge devices. Hayes and Kanan investigated online CL methods using CNN models tailored for embedded devices and provided valuable algorithmic insights. Similarly, Kwon et al. undertook a comparative analysis of rehearsal vs. regularization methods to uncover cost-accuracy trade-offs, including storage, compute, and memory requirements. Ma et al. proposed Miro, an ML platform that dynamically configures key design parameters of CNN-based CL methods to reduce energy costs within the device’s memory capacity. However, none of these studies address the challenges associated with enabling vision transformers for on-device CL, which stands as a main goal of our research.

**Prompting for Continual Learning:** The use of prompts, which are explicit instructions or queries given to the model during training or inference, has shown promise in guiding continual learning for vision transformers [14, 16, 31, 37–39]. The general concept is to fine-tune prompts for new tasks while retaining knowledge acquired from previous tasks. L2P [39] and DualPrompt [38] propose prompt-tuning and prefix-tuning approaches, respectively, by selecting applicable prompts from a shared prompt pool. CODA-Prompt [31] introduces attention-conditioned prompts, which inherently facilitate higher prompting capacity. OVOR [14] uses only a single prompt to expedite the prompt selection stage. Our work suggests three complementary prompting techniques that can benefit all the above methods through full or even partial integration.

### 3. REP: Resource-Efficient Prompting

Prompt-based rehearsal-free CL typically involves two key stages, *prompt selection* and *prompt update*. Figure 1 illustrates an overview of our method REP for making these stages more resource-efficient.

#### 3.1. Prompt Selection

The prompt selection stage operates a neural network model  $f_{\text{query}}$  to extract representations of input data from a prompt pool  $P$ . For a given input  $x_i^j$  in task  $T_i$ ,  $f_{\text{query}}$  calculates a query feature  $q(x_i^j) \in \mathbb{R}^D$  and selects the prompt  $p^*$  that maximizes the cosine similarity between the query and pre-trained prompt  $p_k \in P$ :

$$p^* = \operatorname{argmax}_{p_k \in P} \frac{\langle q(x_i^j), p_k \rangle}{\|q(x_i^j)\| \|p_k\|}. \quad (1)$$

Although  $f_{\text{query}}$  is used only for model inference, its size, typically equivalent to the primary backbone model, can incur a substantial increase in *computation time* and *memory usage*. This is particularly true when it is implemented with a large transformer model. To mitigate these costs, we propose to adopt a more resource-efficient model  $f_{\text{efficient}}$ , which has a smaller depth and width than  $f_{\text{query}}$ .

Simply decreasing one dimension of the model can easily compromise the performance. Thus, we opt for a small pre-trained ViT model (ViT-Ti) as  $f_{\text{efficient}}$ , which we have found proficient in extracting essential representations without excessively cutting down on depth or width. When  $f_{\text{efficient}}$  generates a query feature  $q_{\text{efficient}}(x_i^j) \in \mathbb{R}^d$  (where  $d \leq D$ ), we apply a nonlinear random projection  $\phi$  [25] to maintain the integrity of high-dimensional features in the selected prompt  $p_{\text{efficient}}^*$ , as follows:

$$p_{\text{efficient}}^* = \operatorname{argmax}_{p_k \in P} \frac{\langle \phi(q_{\text{efficient}}(x_i^j)), p_k \rangle}{\|\phi(q_{\text{efficient}}(x_i^j))\| \|p_k\|}. \quad (2)$$

Using ViT-Ti as  $f_{\text{efficient}}$  enables a high level of feature overlap with  $f_{\text{query}}$ . For instance, on Split ImageNet-R, ViT-Ti achieves a prompt overlap of 76.3% on average with ViT-L, the largest  $f_{\text{query}}$  in consideration, based on canonical-correlation analysis (CCA). This leads to nearly identical accuracy between  $f_{\text{efficient}}$  and  $f_{\text{query}}$  (refer to Table 3).

#### 3.2. Prompt Update

The prompt update stage aims to refine learnable parameters for effective training and task adaptability by combining the softmax cross-entropy loss of the classifier  $L_{\text{class}}$  and the cosine similarity loss of the prompt  $L_{\text{prompt}}$ . The combined loss function  $L$  is expressed as:

$$L = L_{\text{class}} \left( f_{\text{update}}(x_i^j), y_i^j \right) + L_{\text{prompt}} \left( p^*, q(x_i^j) \right), \quad (3)$$

where  $f_{\text{update}}$  denotes the backbone model.

#### 3.2.1. Unveiling System-Efficiency Opportunities

Remaining parameters that are not relevant to learnable parameters consist of a number of frozen transformer blocks. Then, are all frozen blocks useful for executing the loss function  $L$ , or can we skip some computations to improve resource efficiency?

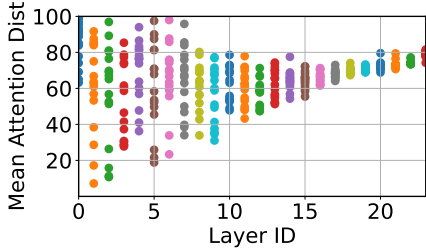
To answer this question, we explore the feature representations of pre-trained transformer blocks with prompts by analyzing the mean attention distance. Mean attention distance reflects the degree to which an attention head focuses on a specific patch relative to others in the input. This metric is widely used to analyze the layer representation of ViT models during the pre-training process [7, 29]. In our study, we re-purpose this concept to examine the behavior of frozen layers during data drift.

For a given head in an attention layer within frozen blocks, let  $(x_0, y_0)$  denote the position of a query patch, and  $(x_i, y_i)$  the positions of patches that the attention head attends to, with corresponding attention weights  $a_i$ . The distance  $d_i$ —typically defined as the Euclidean or pixel distance—is calculated as  $d_i = (x_i - x_0)^2 + (y_i - y_0)^2$ . We then calculate the weighted mean distance as  $\frac{\sum_i a_i \cdot d_i}{\sum_i a_i}$ .

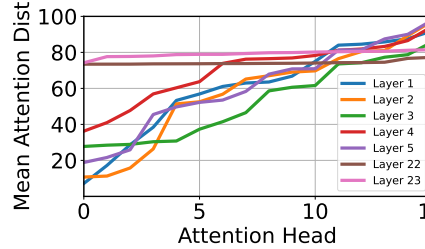
From a continual learning perspective, lower distances indicate a more localized attention pattern, thereby capturing “task-specific” features. Conversely, higher distances reflect a more global attention pattern, aligning with the extraction of more general, “task-agnostic” features. We measure mean attention distances along two dimensions: by layer ID and by attention head. Figure 2 shows these results when adapting to the first task of Split ImageNet-R.

In Figure 2(a), we present analysis results for the pre-trained layer ID using L2P with ViT-L. The lower layers exhibit highly dispersed attention distances, indicating that they simultaneously capture task-specific and task-agnostic information. However, as we examine deeper layers, these distances become increasingly concentrated at higher values, indicating that deeper layers specialize in capturing task-agnostic information. Taking a closer look at attention heads in a few selected layers in Figure 2(b), we observe that attention distances across the heads vary more widely in shallow layers than in deeper layers. Moreover, the lower distances observed in early heads of these shallow layers suggest that the learnable prompts integrated into the model effectively capture task-specific information. This behavior allows the model to retain task-relevant features while progressively specializing deeper layers for more generalized representations.

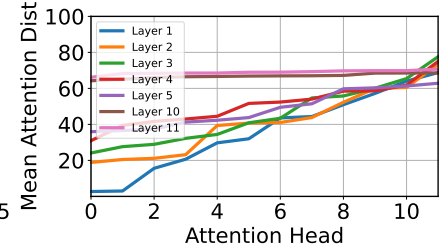
Similar behavior is observed when using DualPrompt with ViT-B in Fig. 2(c). Unlike L2P, DualPrompt integrates prompts directly into the input sequence before the attention layer of each transformer block, rather than only into the first block. This suggests that the feature representations of the pre-trained model, which balance local and global infor-



(a) ViT-L by layer.



(b) ViT-L by attention head.



(c) ViT-B by attention head.

Figure 2. Mean attention distances for frozen blocks along (a) layer IDs and (b/c) attention heads. We run the first task of Split ImageNet-R. (a/b) L2P with ViT-L, and (c) DualPrompt with ViT-B.

mation, may not be greatly affected by the prompt method in use.

Next, we explain how we bring these insights into practice through two compute-skipping techniques.

### 3.2.2. Adaptive Token Merging (AToM)

We first consider the data-efficient compute-skipping method via token merging. Conventional token merging (ToMe) [3] reduces the number of tokens by *uniformly* merging  $n$  redundant tokens per layer, controlled by a fixed scheduler  $r$ . The scheduler function  $r(l) \rightarrow n$  is applied to each layer  $l$ , and according to [3], it merges all tokens, including selected prompts. However, insights from Figure 2 and our additional analysis highlight two major problems.

First, there is a *loss of task-specific information*. The prompt tokens in CL carry essential task-specific information. However, ToMe indiscriminately combines these prompt tokens with others, thereby diminishing their intrinsic value. According to our empirical data in Figure 3, this approach can cause gradient explosions in the prompt tokens, even with gradient clipping, leading to learning instability. Second, there is a *lack of layer-specific adaptability*. Conventional token merging does not account for the disparity between shallow and deep layers, treating all layers uniformly. Therefore, there is a risk of excessive loss of valuable information from shallow layers, which are mainly responsible for adaptability to diverse sequential tasks.

Our *adaptive token merging* (AToM; Algorithm 1) addresses the loss of task-specific information by excluding prompt tokens during token merging, thus maintaining their specificity. To enhance task-specific adaptability, AToM uses a new scheduler  $r'(l) \rightarrow n'$ , which dynamically adjusts the number of tokens to merge based on layer depth, as follows:

$$r'(l) = \min(\delta \times (l - 1), r_{\max}), \quad (4)$$

where  $l$  denotes the layer index,  $\delta$  is the step change in the number of tokens to merge defined as  $\frac{r_{\max}}{L-1}$  (with  $L$  being the number of layers), and  $r_{\max}$  is the maximum number of

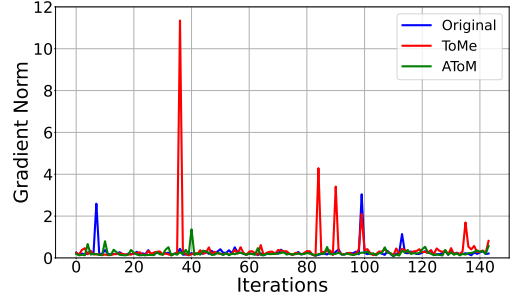


Figure 3. The norm of gradient with respect to the prompt while training Split ImageNet-R when AToM and ToMe (Conventional Token Merging) is applied. ViT-L with L2P is used as a backbone.

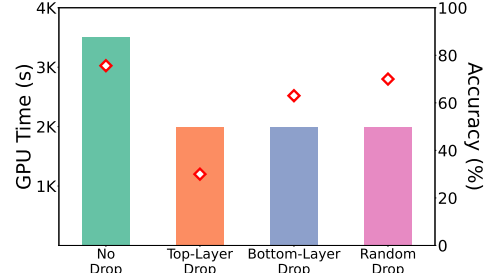


Figure 4. Comparing various layer dropping strategies using L2P with the ViT-L backbone on Split ImageNet-R.

tokens to merge (by default,  $2 \times n$ ). With this  $r'(l)$ , merging occurs more frequently in deeper layers than in shallow layers, preserving important task-related representations.

### 3.2.3. Adaptive Layer Dropping (ALD)

Inspired by insights from Figure 2 and prior work on progressive layer dropping (PLD) [41], we propose *adaptive layer dropping* (ALD; Algorithm 2) with two key features: (1) the dropping schedule considers both temporal and spatial dimensions<sup>1</sup>, and (2) it manages to drop layers non-uniformly to preserve critical task-specific features in shal-

<sup>1</sup>The spatial dimension refers to model layers, each processing input features at different levels of abstraction.

lower layers. On the contrary, PLD only considers the temporal aspect and does not differentiate between layers when dropping. This results in poorer performance compared to ALD, as shown in Table 4.

To strengthen our claim, we conduct a simple experiment that drops 25% of layers from various positions. We compare their training wall-clock GPU time and final average accuracy in Figure 4, using L2P with the ViT-L backbone on Split ImageNet-R. Specifically, Top-layer Drop and Bottom-layer Drop *statically* drop the first and last 25% of layers, respectively, while Random Drop *randomly* skips 25% of layers across the network. For comparison, we also include No Drop, which performs no layer dropping. Although all these naïve strategies incur accuracy loss, Top-layer Drop performs significantly worse than the others. Also, it appears undesirable to bypass only deep layers, even though these layers mainly capture general, task-agnostic features. While Random Drop most closely approaches No Drop’s accuracy, its uniform layer dropping still sacrifices some accuracy. This is why our method ALD carefully accounts for each layer’s spatial aspect in a non-uniform manner to minimize the impact on accuracy.

ALD prioritizes retaining shallow layers that contain richer information essential for model performance, especially after token merging. Thus, instead of operating on its own schedule parameters, ALD leverages feedback from AToM, specifically the count of merged tokens at each layer, to guide layer dropping decisions. The layer-keeping probability  $\theta_{t,l}$  is defined as:

$$\theta_{t,l} = (\alpha(l) \times ((1 - \bar{\theta}) \exp(-\gamma \cdot t) + \bar{\theta})) , \quad (5)$$

where  $\theta_{t,l}$  is the probability of keeping layer  $l$  at time step  $t$ ,  $\bar{\theta}$  is the minimum probability,  $\gamma$  controls the rate of decay, and  $\alpha(l)$  is the adjustment factor for layer  $l$  defined as:

$$\alpha(l) = \begin{cases} \alpha & \text{if } (n(l) - n'(l)) \geq \tau \\ 1 & \text{if } (n(l) - n'(l)) < \tau. \end{cases} \quad (6)$$

$\alpha(l)$  quantifies the degree of token merging performed by AToM in layer  $l$ .  $n(l)$  represents the original number of tokens, and  $n'(l)$  is the number of tokens remaining after merging. When the number of merged tokens surpasses the threshold  $\tau$ , ALD adjusts the layer-dropping probability based on  $\alpha$ . Since deeper layers tend to merge more tokens with AToM, ALD is more likely to exceed  $\tau$  in deeper layers and drop more aggressively. These parameters should be tuned to balance between efficiency and preserving the nuanced information contained in the merged tokens. We set  $\alpha$  to 0.9, and  $\tau$  to 16 for ViT-L, 12 for ViT-B, respectively.

One might contemplate exploiting stochastic depth [13], which gradually increases dropping probabilities for deeper layers without a temporal schedule. We compared ALD and stochastic depth and found that ALD generally offers

1.8–3.3% higher accuracy. This may be attributed to early training iterations after task insertion, which help stabilize training losses [23].

**Resource Efficiency:** REP triggers AToM and ALD for each task insertion to optimize both time and memory usage. Much like our prompt selection optimization, AToM consistently enhances time and memory efficiency. In contrast, ALD solely contributes to reducing time costs because it operates layer-keeping probability  $\theta_{t,l}$  starting at 1.0, *i.e.*, no layer dropping, which necessitates traversing full layers.

## 4. Experiments

We focus on the popular disjoint-CIL setup, where tasks consist of distinct sets of non-overlapping classes and samples from old classes are not given in future tasks [4, 8, 30].

Throughout this section, we will first describe the superiority of ViT-based prompting methods. However, it is important to note that the best-performing method is not fixed and can dynamically change depending on the device memory budget at hand. Therefore, to enhance prompt-based CL for better resource efficiency, we need *adaptive techniques tailored to any backbone* that function regardless of the specific learning method in use. REP is designed for this purpose, and we will evaluate this aspect in detail.

**Data Generation:** To organize task streams, we use three image classification datasets: CIFAR-100 (100 classes) [18], ImageNet-R (200 classes) [12], and PlantDisease (38 classes) [26]. Out of these datasets, ImageNet-R is known for exhibiting much higher intra-class variability among images and an uneven class-size distribution. We divide CIFAR-100 and ImageNet-R into 10 tasks to create **Split CIFAR-100** (*i.e.*, 10 classes per task) and **Split ImageNet-R** (*i.e.*, 20 classes per task), respectively [31, 38, 39]. For PlantDisease, we drop 3 plant disease classes with very few images and organize the remaining 35 classes into 7 tasks to create **Split PlantDisease** (*i.e.*, 5 classes per task).

**Methods:** We employ **L2P** [39], **DualPrompt** [38], and **CODA-Prompt** [31] as representative ViT-based prompting methods. L2P and DualPrompt select suitable prompts via inference, similar to [34], while CODA-Prompt employs a strategy for adaptively optimizing prompts *without* prompt selection, similar to [14]. These methods capitalize on ImageNet pre-trained models as backbones: ViT-L (307M), ViT-B (86M), and ViT-Ti (5.8M)—ViT-Ti is *one of the smallest vision transformer models* to our knowledge. We categorize the prompt-based methods into these three backbone models.

To demonstrate the effectiveness of prompting methods, we also incorporate two state-of-the-art CNN-based methods, **BudgetCL** [6] and **MEMO** [43]. Both BudgetCL and MEMO improve model accuracy by leveraging spare mem-

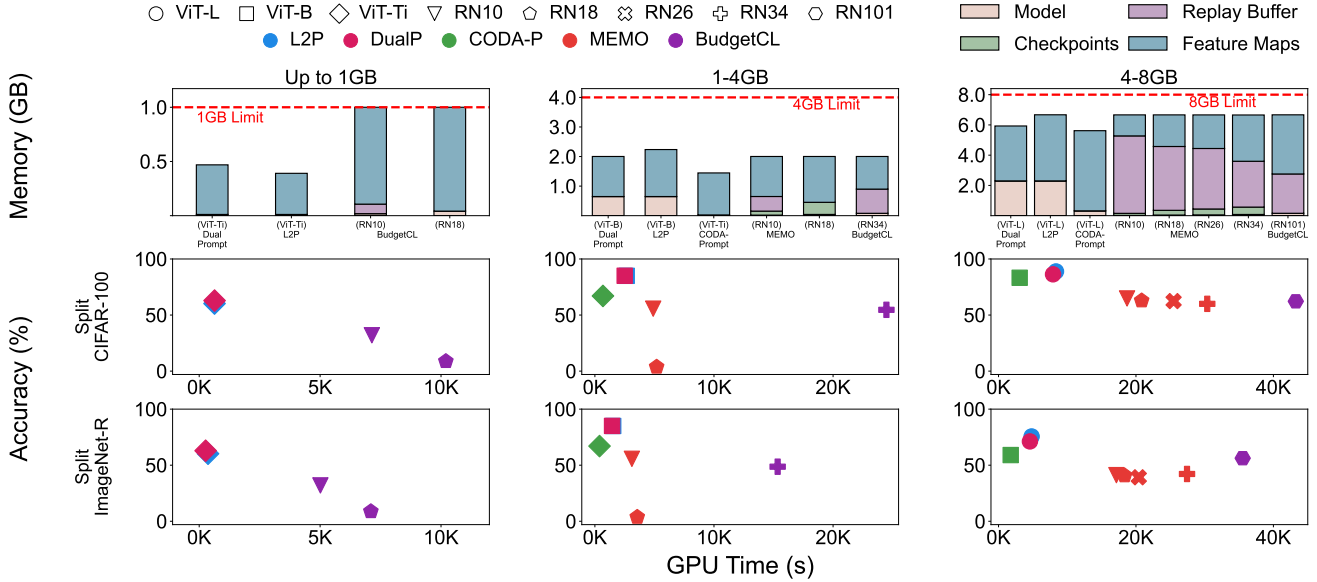


Figure 5. Energy-accuracy trade-offs of various ViT- and CNN-based methods over three different memory budgets: up to 1GB, 1-4GB, and 4-8. The memory breakdown of each method is on the first row. Experiments on Split CIFAR-100 and Split ImageNet-R are on the second and third row, respectively. ViT-based methods consistently outperform CNN-based methods.

ory to store and replay past samples, with MEMO additionally storing model checkpoints from history. These methods also use ImageNet pre-trained models as backbones: ResNet-10 (RN10; 5M), ResNet-18 (RN18; 11M), ResNet-26 (RN26; 14M), ResNet-34 (RN34; 22M), and ResNet-101 (RN101; 43M) models. For fair comparisons, we similarly group methods based on their memory usage. The analysis result is presented in Section 4.1. See Appendix B for detailed settings of all methods mentioned above.

**Hardware and Metrics:** We use NVIDIA RTX 3090 as a reference GPU to cover a wide range of memory sizes while maintaining consistent computational power and measure the GPU iteration time required for computation—GPU iteration time can be correlated *linearly* with energy usage [23]. In Appendix H, we evaluate our memory-efficient method directly on NVIDIA Jetson TX2, although it is applicable beyond this specific device. We also report the final average accuracy by averaging the accuracy of all classes after the last task training [5, 31], which assesses the decline in task accuracy averaged over all tasks.

#### 4.1. Preliminary Empirical Study

We first uncover the *energy-accuracy trade-offs* to highlight the impact of each baseline method on the accuracy gained relative to its training cost. Figure 5 visually represents the comparison results across device memory capacities and datasets. In each graph, the x-axis indicates wall-clock time, which corresponds to energy cost (lower is better), while the y-axis indicates final average accuracy (higher is better). Thus, a more cost-effective method appears closer to the

upper-left corner of the graph. Overall, ViT-based methods outperform CNN-based methods by a large margin, achieving 26–36% higher accuracy with 45–90% less time and energy spent under the same memory budget. We elaborate on two key characteristics that explain these results:

**Scaling Across Varying Backbone Networks.** ViT-based methods scale well, with larger backbone networks overall yielding higher accuracy. In contrast, CNN-based methods scale poorly with increased backbone size. Specifically, on Split ImageNet-R, a more challenging dataset, MEMO/RN34 is only 2.95% better than MEMO/RN18, despite being around twice larger. On Split CIFAR-100, increasing the backbone size yields only limited gains.

**Memory Efficiency.** CNN-based methods are often considered more memory-efficient because they use backbones a magnitude smaller than ViT models. Thus, it is commonly believed that ample memory can be allocated to replay samples or past model checkpoints [43], which help improve model performance. However, in CL, which involves typical training iterations, a substantial amount of memory must be allocated for feature maps [22], leaving little room for memory buffers. For instance, for a device memory range of 1–4GB in Table 1, the backbone of MEMO/RN18 consumes only 43MB of memory (6.5% of ViT-L), but feature maps occupy as much as 1.7GB (more than ViT-based methods). This causes MEMO/RN18 to be short on memory for the replay buffer, dramatically degrading model accuracy, as observed in Figure 5.

Table 2. Accuracy and computational cost of all competing methods on Split CIFAR-100, Split ImageNet-R, and Split PlantDisease datasets. We report *Final Average Accuracy* (Acc.) both without and with REP. Iteration time (ms) and memory usage (GB) are provided in absolute terms, along with their percentage values relative to REP. (↑) higher is better, (↓) lower is better.

Model	Method	Split CIFAR-100		Split ImageNet-R		Split PlantDisease		Iter. time (ms)		Mem. (GB)	
		Acc. (↑)	w/ REP	Acc. (↑)	w/ REP	Acc. (↑)	w/ REP	Iter.time (↓)	w/ REP	Mem. (↓)	w/ REP
ViT-L	L2P	88.2±0.3	86.4±0.3	75.6±1.0	75.3±0.9	75.9±3.1	81.1±3.9	446.9	235.4 (-47.3%)	6.5	4.5 (-31.5%)
	DualPrompt	86.3±0.3	84.5±0.6	71.2±0.6	70.6±0.9	75.1±1.1	78.2±2.9	423.7	202.5 (-52.2%)	5.9	4.3 (-27.8%)
	CODA-Prompt	85.4±0.4	83.7±0.8	74.4±0.6	72.4±0.9	75.0±2.0	74.0±2.7	568.0	431.1 (-24.1%)	13.2	11.0 (-16.8%)
	UpperBound	94.1±0.1	-	85.2±0.2	-	99.6±0.3	-	426.7	-	9.8	-
ViT-B	L2P	84.5±0.8	83.4±1.8	59.4±0.8	59.7±1.2	64.4±2.6	64.0±2.4	142.5	100.1 (-29.8%)	2.3	2.0 (-11.8%)
	DualPrompt	85.1±0.2	84.9±0.9	68.1±0.1	67.0±1.0	78.0±1.5	77.0±1.8	133.4	99.7 (-25.2%)	2.1	1.8 (-11.2%)
	CODA-Prompt	83.3±0.9	81.3±1.9	59.0±0.3	58.0±1.7	71.4±0.8	70.2±2.7	164.1	144.8 (-11.8%)	6.9	5.7 (-17.8%)
	UpperBound	92.0±0.2	-	81.4±0.1	-	99.6±0.4	-	143.2	-	3.2	-
ViT-Ti	L2P	60.3±0.2	58.9±1.3	41.2±0.7	40.3±1.0	56.1±2.9	55.0±2.8	33.8	29.0 (-14.2%)	0.5	0.5 (-2.1%)
	DualPrompt	62.9±0.5	62.5±0.9	43.6±0.8	42.7±1.0	64.0±1.0	61.9±1.8	33.9	30.0 (-11.6%)	0.4	0.4 (-4.8%)
	CODA-Prompt	67.0±0.4	65.9±1.8	49.3±0.8	47.6±2.0	66.8±0.8	65.0±2.6	36.1	29.8 (-17.4%)	2.8	2.8 (-0.7%)
	UpperBound	83.0±0.1	-	77.4±0.2	-	98.0±0.9	-	42.3	-	0.6	-

## 4.2. Main Results

Table 2 presents the efficacy of REP when integrated into prompt-based CL methods across various ViT backbones (ViT-L, ViT-B, ViT-Ti) and datasets.

**Resource Efficiency:** Integrating REP into existing prompt-based CL methods significantly reduces computational overhead and memory usage across all model configurations: we observe memory savings of up to 32% for ViT-L, 18% for ViT-B, and 5% for ViT-Ti.

Although the backbone network parameters remain frozen during training, the model must still perform a backward pass to compute losses for both classification and prompt learning. As a result, a substantial amount of memory is allocated to store intermediate activations. By selectively merging tokens (AToM) and adaptively dropping layers (ALD), REP mitigates these memory demands without compromising performance-critical information flow.

The advantages of REP extend to training speed, which is closely linked to energy consumption. For ViT-L, the largest architecture considered, REP reduces iteration time by up to 52% compared to baseline methods, translating directly into lower energy consumption. In contrast, with the more compact ViT-Ti backbone, resource savings persist but are less pronounced due to the model’s already low computational cost. These results highlight the versatility of REP, demonstrating its scalability from compact to large models while ensuring substantial resource efficiency gains across different regimes.

**Accuracy:** While L2P, DualPrompt, and CODA-Prompt were originally designed and evaluated on a ViT-B backbone, our study systematically extends these methods across a diverse range of ViT architectures, considering their energy-accuracy trade-offs in on-device CL under var-

ious memory constraints. This broader perspective reveals notable gains in resource efficiency with REP, archived with only marginal accuracy drops, e.g., 0.03–1.36% on Split CIFAR-100 and 0.26–1.62% on Split ImageNet-R. In some cases, accuracy even improves. For instance, on ViT-L with Split PlantDisease, L2P’s accuracy increases from 75.92% to 81.08% when REP is applied. These findings suggest that AToM and ALD effectively eliminate redundant computations while preserving essential features for CL.

## 4.3. Ablation and Additional Study

We validate our proposed techniques and algorithm designs along with the chosen hyperparameters. The study here primarily uses the ViT-L backbone on Split ImageNet-R, where L2P is the best non-optimized method.

**Component Ablation:** In Table 3, we ablate REP’s components to assess their contributions to resource efficiency. Each component plays a key role in reducing memory and compute time, with ALD affecting compute time only, as expected. Notably, AToM substantially optimizes both resource usages.

**Algorithm Validation:** Token merging (ToMe) [3] and progressive layer dropping (PLD) [41] are specifically designed to accelerate traditional transformer-based model training. To validate the importance of incorporating our adaptive techniques instead in CL, we evaluate how REP performs in case AToM and ALD are replaced with ToMe and PLD, respectively. The results are presented in Table 4. Although applying ToMe or PLD improves system efficiency over L2P, it results in an accuracy loss of 5.15% or 2.01%, respectively, compared to using our techniques. This indicates that ToMe and PLD are less desirable for achieving our goal, i.e., enhancing system efficiency without compromising accuracy.

Table 3. Ablation study of REP components, demonstrating their contributions to both resource efficiency and accuracy.

Ablated components	Acc. ( $\uparrow$ )	Fgt. ( $\downarrow$ )	GPU Time (s)	Mem. (GB)
REP (ours)	75.6 $\pm$ 1.0	3.6 $\pm$ 0.3	2542.4	4.5
(1) $f_{\text{efficient}}$	74.8 $\pm$ 0.8	4.0 $\pm$ 0.8	3698.8	5.5
(2) AToM	74.9 $\pm$ 0.8	3.5 $\pm$ 0.8	4442.0	5.6
(3) ALD	74.5 $\pm$ 0.8	3.6 $\pm$ 0.7	4244.0	6.7
(4) $f_{\text{efficient}}$ + AToM	74.2 $\pm$ 0.8	4.0 $\pm$ 0.8	2861.4	4.5
(5) $f_{\text{efficient}}$ + ALD	74.5 $\pm$ 0.4	3.4 $\pm$ 0.5	3206.7	5.5
(6) AToM + ALD	74.6 $\pm$ 0.4	2.6 $\pm$ 0.5	3448.8	4.8

Table 4. Accuracy of using traditional token merging (ToMe) or layer dropping (PLD) instead of our adaptive algorithms.

	Acc. ( $\uparrow$ )	Fgt. ( $\downarrow$ )	GPU Time (s)	Mem. (GB)
REP (ours)	75.6 $\pm$ 1.0	3.6 $\pm$ 0.3	2542.4	4.5
(1) w/ ToMe	70.2 $\pm$ 0.7	2.6 $\pm$ 0.9	2917.8	3.7
(2) w/ PLD	73.3 $\pm$ 0.7	3.9 $\pm$ 0.7	2741.9	4.5

Table 5. REP over different # of merged tokens ( $n$ ) and % of keep ratio ( $\theta$ ). We use  $n = 8$  and  $\theta = 0.5$  as default values.

$n$ (w/ $\theta=0.5$ )	Acc. ( $\uparrow$ )	Fgt. ( $\downarrow$ )	GPU Time (s)	Mem. (GB)
2	76.2 $\pm$ 0.7	3.5 $\pm$ 0.7	2808.4	5.5
4	75.3 $\pm$ 0.3	3.3 $\pm$ 0.5	2714.0	5.2
8	75.6 $\pm$ 0.9	3.6 $\pm$ 0.3	2542.4	4.5
$\theta$ (w/ $n=8$ )	Acc. ( $\uparrow$ )	Fgt. ( $\downarrow$ )	GPU Time (s)	Mem. (GB)
0.25	73.2 $\pm$ 0.6	4.0 $\pm$ 0.5	2362.1	4.5
0.50	75.6 $\pm$ 1.0	3.6 $\pm$ 0.3	2542.4	4.5
0.75	74.4 $\pm$ 0.6	3.5 $\pm$ 0.5	2861.4	4.5

**AToM and ALD Intensity:** Table 5 shows the effects of varying intensities of AToM and ALD, focusing on the number of merged tokens ( $n$ ) in AToM and the keep ratio ( $\theta$ ) in ALD. AToM appears to maintain stable accuracy even as more tokens are merged. In contrast, for ALD, a lower keep ratio improves system efficiency by reducing iteration time and memory usage, but it can markedly impair model accuracy if the ratio is too low. Overall, when used with caution, AToM and ALD can effectively balance system efficiency and accuracy.

## 5. Conclusion

In this work, we introduced Resource-Efficient Prompting (REP), a framework designed to enhance the computational and memory efficiency of prompt-based rehearsal-free continual learning methods. By incorporating adaptive token merging and adaptive layer dropping, REP selectively streamlines the learning process while preserving

task-specific features, significantly reducing resource consumption without compromising accuracy. Experiments on multiple image classification datasets demonstrate that REP achieves substantial efficiency gains over state-of-the-art ViT- and CNN-based methods, making it a practical solution for on-device continual learning.

Since our study focuses on scenarios wherein a sequence of tasks is presented within learning environments, our method does not determine the *curriculum* of learning. Future work could extend our method for curriculum-based continual learning. Moreover, although using replay buffer may not be feasible in real-world scenarios due to data privacy concerns, on-device CL is already viewed as a privacy-preserving approach, making rehearsal-based REP a promising direction.

## References

- [1] Saad Ahmed, Bashima Islam, Kasim Sinan Yildirim, Marco Zimmerling, Przemysław Pawełczak, Muhammad Hamad Alizai, Brandon Lucia, Luca Mottola, Jacob Sorber, and Josiah Hester. The Internet of Batteryless Things. *CACM*, 67(3):64–73, 2024. [1](#)
- [2] Jihwan Bang, Heesu Kim, YoungJoon Yoo, Jung-Woo Ha, and Jonghyun Choi. Rainbow Memory: Continual Learning with a Memory of Diverse Samples. In *CVPR*, 2021. [2](#)
- [3] Daniel Bolya, Cheng-Yang Fu, Xiaoliang Dai, Peizhao Zhang, Christoph Feichtenhofer, and Judy Hoffman. Token Merging: Your ViT But Faster. In *ICLR*, 2023. [4](#), [7](#), [14](#)
- [4] Francisco M. Castro, Manuel J. Marin-Jimenez, Nicolas Guil, Cordelia Schmid, and Karteek Alahari. End-to-End Incremental Learning. In *ECCV*, 2018. [2](#), [5](#)
- [5] Arslan Chaudhry, Puneet K. Dokania, Thalaiyasingam Ajanthan, and Philip H. S. Torr. Riemannian Walk for Incremental Learning: Understanding Forgetting and Intransigence. In *ECCV*, 2018. [2](#), [6](#)
- [6] Arslan Chaudhry, Marcus Rohrbach, Mohamed Elhoseiny, Thalaiyasingam Ajanthan, Puneet K. Dokania, Philip HS Torr, and Marc’Aurelio Ranzato. On Tiny Episodic Memories in Continual Learning. *arXiv:1902.10486*, 2019. [5](#)
- [7] Alexey Dosovitskiy, Lucas Beyer, Alexander Kolesnikov, Dirk Weissenborn, Xiaohua Zhai, Thomas Unterthiner, Mostafa Dehghani, Matthias Minderer, Georg Heigold, Sylvain Gelly, Jakob Uszkoreit, and Neil Houlsby. An Image is

Worth 16x16 Words: Transformers for Image Recognition at Scale. In *ICLR*, 2021. 3

[8] Alexander Gepperth and Barbara Hammer. Incremental Learning Algorithms and Applications. In *ESANN*, 2016. 2, 5

[9] In Gim and JeongGil Ko. Memory-Efficient DNN Training on Mobile Devices. In *MobiSys*, 2022. 2

[10] Tyler L Hayes and Christopher Kanan. Online Continual Learning for Embedded Devices. In *CoLLAs*, 2022. 1, 2

[11] Kaiming He, Xiangyu Zhang, Shaoqing Ren, and Jian Sun. Deep Residual Learning for Image Recognition. In *CVPR*, 2016. 16

[12] Dan Hendrycks, Steven Basart, Norman Mu, Saurav Kadavath, Frank Wang, Evan Dorundo, Rahul Desai, Tyler Zhu, Samyak Parajuli, Mike Guo, Dawn Song, Jacob Steinhardt, and Justin Gilmer. The Many Faces of Robustness: A Critical Analysis of Out-of-Distribution Generalization. In *ICCV*, 2021. 5, 13

[13] Gao Huang, Yu Sun, Zhuang Liu, Daniel Sedra, and Kilian Q Weinberger. Deep Networks with Stochastic Depth. In *ECCV*, 2016. 5

[14] Wei-Cheng Huang, Chun-Fu Chen, and Hsiang Hsu. OVOR: OnePrompt with Virtual Outlier Regularization for Rehearsal-Free Class-Incremental Learning. In *ICLR*, 2024. 2, 5, 18

[15] Seunghyeok Jeon, Yonghun Choi, Yeonwoo Cho, and Ho-jung Cha. HarvNet: Resource-Optimized Operation of Multi-Exit Deep Neural Networks on Energy Harvesting Devices. In *MobiSys*, 2023. 1

[16] Dahuin Jung, Dongyoon Han, Jihwan Bang, and Hwanjun Song. Generating Instance-level Prompts for Rehearsal-free Continual Learning. In *ICCV*, 2023. 1, 2

[17] Diederik P. Kingma and Jimmy Ba. Adam: A Method for Stochastic Optimization. In *ICLR*, 2015. 12

[18] Alex Krizhevsky and Geoffrey Hinton. Learning Multiple Layers of Features from Tiny Images. *Master's thesis, Department of Computer Science, University of Toronto*, 2009. 5, 13

[19] Jaecheon Kwak, Sunjae Lee, Dae R Jeong, Arjun Kumar, Dongjae Shin, Ilju Kim, Donghwa Shin, Kilho Lee, Jinkyu Lee, and Insik Shin. MixMax: Leveraging Heterogeneous Batteries to Alleviate Low Battery Experience for Mobile Users. In *MobiSys*, 2023. 1

[20] Young D Kwon, Jagmohan Chauhan, Abhishek Kumar, Pan Hui HKUST, and Cecilia Mascolo. Exploring System Performance of Continual Learning for Mobile and Embedded Sensing Applications. In *IEEE/ACM SEC*, 2021. 1, 2

[21] Soobee Lee, Minindu Weerakoon, Jonghyun Choi, Minjia Zhang, Di Wang, and Myeongjae Jeon. CarM: Hierarchical Episodic Memory for Continual Learning. In *DAC*, 2022. 2

[22] Gangmuk Lim, Jeongseob Ahn, Wencong Xiao, Youngjin Kwon, and Myeongjae Jeon. Zico: Efficient GPU Memory Sharing for Concurrent DNN Training. In *USENIX ATC*, 2021. 6

[23] Xinyue Ma, Suyeon Jeong, Minjia Zhang, Di Wang, Jonghyun Choi, and Myeongjae Jeon. Cost-effective On-device Continual Learning over Memory Hierarchy with Miro. In *MobiCom*, 2023. 1, 2, 5, 6, 15, 16

[24] Michael McCloskey and Neal J. Cohen. Catastrophic Interference in Connectionist Networks: The Sequential Learning Problem. In *Psychol. Learn. Motiv. - Adv. Res. Theory*, 1989. 1

[25] Mark D McDonnell, Dong Gong, Amin Parvaneh, Ehsan Abbasnejad, and Anton van den Hengel. Random Projection in Deep Neural Networks. In *NeurIPS*, 2024. 3

[26] Sharada Prasanna Mohanty, David Hughes, and Marcel Salathe. Using Deep Learning for Image-Based Plant Disease Detection. *arXiv:1604.0316*, 2016. 5, 13, 14

[27] Ameya Prabhu, Philip HS Torr, and Puneet K Dokania. GDumb: A Simple Approach that Questions Our Progress in Continual Learning. In *ECCV*, 2020. 2

[28] Ameya Prabhu, Hasan Abed Al Kader Hammoud, Puneet K. Dokania, Philip H.S. Torr, Ser-Nam Lim, Bernard Ghanem, and Adel Bibi. Computationally Budgeted Continual Learning: What Does Matter? In *CVPR*, 2023. 2

[29] Maithra Raghu, Thomas Unterthiner, Simon Kornblith, Chiyuan Zhang, and Alexey Dosovitskiy. Do Vision Transformers See Like Convolutional Neural Networks? In *NeurIPS*, 2021. 3

[30] Sylvestre-Alvise Rebuffi, Alexander Kolesnikov, Georg Sperl, and Christoph H. Lampert. iCaRL: Incremental Classifier and Representation Learning. In *CVPR*, 2017. 2, 5

[31] James Seale Smith, Leonid Karlinsky, Vyshnavi Gutta, Paola Cascante-Bonilla, Donghyun Kim, Assaf Arbelle, Rameswar Panda, Rogerio Feris, and Zsolt Kira. CODA-Prompt: COntinual Decomposed Attention-based Prompting for Rehearsal-Free Continual Learning. In *CVPR*, 2023. 1, 2, 5, 6, 12, 16, 18

[32] Andreas Peter Steiner, Alexander Kolesnikov, Xiaohua Zhai, Ross Wightman, Jakob Uszkoreit, and Lucas Beyer. How to train your ViT? Data, Augmentation, and Regularization in Vision Transformers. *TMLR*, 2022. 1

[33] C. Wah, S. Branson, P. Welinder, P. Perona, and S. Belongie. Caltech-UCSD Birds 200. Technical Report CNS-TR-2011-001, Caltech, 2011. 13

[34] Liyuan Wang, Jingyi Xie, Xingxing Zhang, Mingyi Huang, Hang Su, and Jun Zhu. Hierarchical Decomposition of Prompt-Based Continual Learning: Rethinking Obscured Sub-optimality. In *NeurIPS*, 2023. 5, 17

[35] Qipeng Wang, Mengwei Xu, Chao Jin, Xinran Dong, Jiliang Yuan, Xin Jin, Gang Huang, Yunxin Liu, and Xuanzhe Liu. Melon: Breaking the Memory Wall for Resource-Efficient on-Device Machine Learning. In *MobiSys*, 2022. 2

[36] Yue Wang, Ziyu Jiang, Xiaohan Chen, Pengfei Xu, Yang Zhao, Yingyan Lin, and Zhangyang Wang. E2-Train: Training State-of-the-art CNNs with Over 80% Energy Savings. In *NeurIPS*, 2019. 2

[37] Yabin Wang, Zhiwu Huang, and Xiaopeng Hong. S-Prompts Learning with Pre-trained Transformers: An Occam's Razor for Domain Incremental Learning. In *NeurIPS*, 2022. 1, 2

[38] Zifeng Wang, Zizhao Zhang, Sayna Ebrahimi, Ruoxi Sun, Han Zhang, Chen-Yu Lee, Xiaoqi Ren, Guolong Su, Vincent Perot, Jennifer Dy, and Tomas Pfister. DualPrompt: Complementary Prompting for Rehearsal-Free Continual Learning. In *ECCV*, 2022. 1, 2, 5, 12, 16

- [39] Zifeng Wang, Zizhao Zhang, Chen-Yu Lee, Han Zhang, Ruoxi Sun, Xiaoqi Ren, Guolong Su, Vincent Perot, Jennifer Dy, and Tomas Pfister. Learning To Prompt for Continual Learning. In *CVPR*, 2022. [1](#), [2](#), [5](#), [11](#), [12](#)
- [40] Dianlei Xu, Tong Li, Yong Li, Xiang Su, Sasu Tarkoma, Tao Jiang, Jon Crowcroft, and Pan Hui. Edge Intelligence: Architectures, Challenges, and Applications. *arXiv:2003.12172*, 2020. [1](#)
- [41] Minjia Zhang and Yuxiong He. Accelerating Training of Transformer-Based Language Models with Progressive Layer Dropping. In *NeurIPS*, 2020. [4](#), [7](#), [14](#)
- [42] Yuqing Zhao, Divya Saxena, and Jannong Cao. Memory-Efficient Domain Incremental Learning for Internet of Things. In *SenSys*, 2023. [1](#)
- [43] Da-Wei Zhou, Qi-Wei Wang, Han-Jia Ye, and De-Chuan Zhan. A Model or 603 Exemplars: Towards Memory-Efficient Class-Incremental Learning. In *ICLR*, 2023. [2](#), [5](#), [6](#), [12](#), [13](#)
- [44] Da-Wei Zhou, Zi-Wen Cai, Han-Jia Ye, De-Chuan Zhan, and Ziwei Liu. Revisiting Class-Incremental Learning with Pre-Trained Models: Generalizability and Adaptivity are All You Need. *IJCV*, 2024. [17](#)

## A. Algorithm Details

---

**Algorithm 1** Adaptive Token Merging (AToM)

---

**Input:** Initial set of all tokens  $T$ ; Set of prompt tokens  $P$ ;  
 Number of model layers  $L$ ;  
 Maximum number of tokens to merge  $r_{\max}$   
**Initialize:**  $T'_{\text{final}} \leftarrow T$ ;

- 1: **for**  $l \in \{1, 2, \dots, L\}$  **do**
- 2:    $T_{\text{attn}} \leftarrow \text{MSA}(T'_{\text{final}})$
- 3:    $T_{\text{eligible}} \leftarrow T_{\text{attn}} \setminus P$
- 4:    $\delta \leftarrow \frac{r_{\max}}{L-1}$
- 5:    $n' \leftarrow \min(\delta \times (l-1), r_{\max})$
- 6:    $T'_{\text{merged}} \leftarrow \text{Merge}(T_{\text{eligible}}, n')$
- 7:    $T_{\text{concat}} \leftarrow \text{Concat}(T'_{\text{merged}}, P)$
- 8:    $T'_{\text{final}} \leftarrow \text{MLP}(T_{\text{concat}}, l)$
- 9: **end for**
- 10: **return**  $T'_{\text{final}}$

---

**Algorithm 2** Adaptive Layer Dropping (ALD)

---

**Input:** Input tensor  $X$ ; Keep ratio of layer  $\theta_{t,l}$ ;  
 Number of layers  $L$ ; Minimum ratio  $\bar{\theta}$ ;  
 Decay rate  $\gamma$ ; Spatial threshold  $\tau$ ;  
 Adjustment factor  $\alpha$

- 1: **for**  $l \in \{1, 2, \dots, L\}$  **do**
- 2:   **if**  $(n(l) - n'(l)) > \tau$  **then**
- 3:      $\alpha(l) \leftarrow \alpha$
- 4:   **else**
- 5:      $\alpha(l) \leftarrow 1$
- 6:   **end if**
- 7:    $\theta_{t,l} \leftarrow \alpha(l) \times ((1 - \bar{\theta}) \exp(-\gamma \cdot t) + \bar{\theta})$
- 8:   **if**  $\text{Bernoulli}(\theta_{t,l}) = 1$  **then**
- 9:      $X_{\text{out}} \leftarrow \text{Exec}(l, X_{\text{out}})$
- 10:   **else**
- 11:      $X_{\text{out}} \leftarrow X_{\text{out}}$
- 12:   **end if**
- 13: **end for**
- 14: **return**  $X_{\text{out}}$

---

## B. Implementation Details

Unless otherwise stated, we use the term **REP-L** to denote REP applied to L2P with a ViT-L backbone, which stands out as the best-performing baseline method for Split CIFAR-100 and Split ImageNet-R within the 4–8GB memory range. Similarly, the notations **L**, **B**, and **Ti** are used to generally denote **ViT-L**, **ViT-B**, and **ViT-Ti** backbones, respectively, in the prompt update stage of any prompt-based method.

### B.1. Prompt-Based Methods for REP

We present details on the three major prompt-based methods to which REP is integrated for resource efficiency.

**Learning to Prompt (L2P)** positions prompts at the first layer of the transformer architecture [39]. These prompts are learnable parameters that dynamically evolve with the training process. The mechanism begins with a prompt pool  $P = \{p_1, p_2, \dots, p_m\} \subset \mathbb{R}^{L_p \times D}$ .

For a given input  $x_i^j$  in task  $T_i$ , L2P computes a query feature  $q(x_i^j) \in \mathbb{R}^D$  to select the corresponding prompt. The prompt  $p^*$  is selected based on maximizing the cosine similarity with respect to the query:

$$p^* = \operatorname{argmax}_{p_k \in P} \sum_{c=1}^{L_p} \frac{\langle q(x_i^j), [p_k]_{(c,:)}^\top \rangle}{\|q(x_i^j)\| \| [p_k]_{(c,:)}^\top \|}, \quad (7)$$

where  $[p_k]_{(c,:)}$  is the  $c$ -th row of  $p_k$ .

The selected prompt  $p^*$  is concatenated with the input embedding  $z(x_i^j)$  to form the prompt-augmented input  $z'(x_i^j) = [p^*; z(x_i^j)]$ . The training objective of L2P balances classification loss  $L_{\text{class}}$  and prompt-adjustment loss  $L_{\text{prompt}}$ :

$$L = L_{\text{class}}(z'(x_i^j), y_i^j) + L_{\text{prompt}}(p^*, q(x_i^j)). \quad (8)$$

**DualPrompt** leverages prompts at multiple layers of the transformer architecture [38]. It introduces a general prompt  $g \in \mathbb{R}^{L_g \times D}$  and a set of task-specific prompts  $E = \{e_1, e_2, \dots, e_T\} \subset \mathbb{R}^{L_e \times D}$ . These prompts are incorporated at specified layers in the transformer model.

For a given input  $x_i^j$  in task  $T_i$ , the model's transformer layers  $f$  are modified by attaching  $g$  and  $e_i$  to the layers, resulting in a prompted architecture  $f_{g,e_i}$ . The feature transformation  $h_i^j$  for the input sample  $x_i^j$  is then obtained as:

$$h_i^j = f_{g,e_i}(x_i^j). \quad (9)$$

Similar to L2P, DualPrompt optimizes  $L_{\text{class}}$  and  $L_{\text{prompt}}$ :

$$L = L_{\text{class}}(h_i^j, y_i^j) + L_{\text{prompt}}(g, e_i). \quad (10)$$

**CODA-Prompt** decomposes learnable prompts into components and uses an attention mechanism from a pre-trained ViT model to select relevant prompts [31]. Instead of a single prompt, CODA-Prompt learns a set of prompt components  $P = \{P_1, P_2, \dots, P_M\}$ . The final prompt  $p$  is a weighted sum:

$$p = \sum_m \alpha_m P_m, \quad (11)$$

where weights  $\alpha$  are determined based on the query  $q(x)$  and keys  $K \in \mathbb{R}^{D \times M}$ :

$$\alpha = \gamma(q(x), K). \quad (12)$$

When the task changes, the current components are frozen, and new one is added, promoting orthogonality:

$$L_{\text{ortho}}(B) = \|BB^\top - I\|^2, \quad (13)$$

where  $B$  represents  $P$ ,  $K$ , or  $A$  ( $A$  represents the *attention vector*). The full optimization target is:

$$\min_{P^n, K^n, A^n, \phi^n} L(f_\phi(f_{\theta, P, K, A}(x)), y) + \lambda (L_{\text{ortho}}(P) + L_{\text{ortho}}(K) + L_{\text{ortho}}(A)) \quad (14)$$

where  $P^n$ ,  $K^n$ , and  $A^n$  are new components, and  $\lambda$  balances the orthogonality loss [31].

## B.2. Hyperparameters and Configurations

For all prompt-based CL methods, we employ the ADAM optimizer [17] configured with hyperparameters  $\beta_1 = 0.99$  and  $\beta_2 = 0.999$ . In contrast, BudgetCL and MEMO adopt the stochastic gradient descent (SGD) optimizer with a momentum coefficient of 0.9 and a weight decay of 0.002, both validated as effective by similar replay buffer-based methods [39]. In REP, we set the prompt pool size to 10 and the prompt length to 5, following the original implementations of L2P<sup>2</sup> and DualPrompt.<sup>3</sup> The learning rate for the prompt-based methods is set to 0.001875. For CODA-Prompt, we implement a cosine decay learning rate strategy, as outlined in its original paper [31]. For BudgetCL and MEMO, the learning rate is set to 0.1 and decays by 0.1 at 80 and 150 epochs following the original paper [43].

<sup>2</sup>L2P PyTorch Implementation. <https://github.com/JH-LEE-KR/l2p-pytorch>.

<sup>3</sup>DualPrompt PyTorch Implementation. <https://github.com/JH-LEE-KR/dualprompt-pytorch>.

Table 6. Results on Split CIFAR-100, with ViT-B as the backbone model (following the original setups).

Method	Acc. ( $\uparrow$ )	Fgt. ( $\downarrow$ )	GPU Time (s)	Mem. (GB)
REP-L (ours)	86.89 $\pm$ 0.57	4.65 $\pm$ 0.14	4420.99	4.45
L2P-B	84.36 $\pm$ 0.68	7.35 $\pm$ 0.38	2802.42	14.20
DualPrompt-B	85.27 $\pm$ 0.75	5.16 $\pm$ 0.09	2624.06	12.30
CODA-Prompt-B	86.09 $\pm$ 0.73	1.67 $\pm$ 0.26	3226.58	18.83

Table 7. Results on Split ImageNet-R, with ViT-B as the backbone model (following the original setups).

Method	Acc. ( $\uparrow$ )	Fgt. ( $\downarrow$ )	GPU Time (s)	Mem. (GB)
REP-L (ours)	75.34 $\pm$ 0.16	3.58 $\pm$ 0.29	2542.43	4.45
L2P-B	59.66 $\pm$ 0.81	9.73 $\pm$ 0.47	1609.88	14.20
DualPrompt-B	67.45 $\pm$ 0.88	4.68 $\pm$ 0.20	1507.42	12.30
CODA-Prompt-B	75.52 $\pm$ 0.74	1.64 $\pm$ 0.10	1853.54	18.83

Table 8. Results on Split CUB-200, with ViT-L as the backbone model.

Method	Acc. ( $\uparrow$ )	Fgt. ( $\downarrow$ )	GPU Time (s)	Mem. (GB)
REP-L (ours)	74.70 $\pm$ 1.04	6.67 $\pm$ 0.34	529.67	4.45
L2P-L	74.70 $\pm$ 1.02	6.68 $\pm$ 1.35	1005.57	6.67
DualPrompt-L	72.35 $\pm$ 0.98	7.82 $\pm$ 0.31	953.42	5.93
CODA-Prompt-L	79.46 $\pm$ 0.84	5.84 $\pm$ 0.99	1257.82	13.95

We consistently use the mini-batch size of 16 for all methods to maintain a uniform computational load for each training iteration. For fair comparisons, each method performs 1875, 1080, and 2583 iterations per task insertion for Split CIFAR-100 [18], Split ImageNet-R [12], and Split PlantDisease [26], respectively. This setup ensures that among prompt-based methods, iteration time itself correlates linearly with energy usage, as training wall-clock time similarly reflects energy consumption as discussed in the main paper.

BudgetCL and MEMO select 8 samples from the new task and another 8 samples from old tasks in the replay buffer to organize 16 samples in each mini-batch. We adopt the setup in [43] and train 200 epochs for all datasets used. Thus, BudgetCL and MEMO perform more iterations per epoch for a bigger replay buffer, translating into longer GPU time and more energy usage.

## C. Competing Methods with Original Setups

For the evaluation of L2P, DualPrompt, and CODA-Prompt in the main paper, we adhere to the hyperparameters specified in the original studies, except for the *number of iterations per task* and *batch size*. We adopt a smaller batch size to account for on-device memory limitations, which prevent the use of the original batch sizes. Nonetheless, we present the results of these three methods using their original hyperparameters in Table 6 and Table 7, respectively. Although these methods are based on the ViT-B backbone, they consume significantly more memory than REP-L (with the ViT-L backbone), primarily due to their originally large batch sizes.

## D. Additional Datasets

We also expand our experiments on REP by incorporating an additional dataset: Split CUB-200 [33], which is designed for fine-grained image classification. Split CUB-200 contains 5,994 bird images categorized into 200 classes, which are split into 5 CL tasks, each having 40 classes. We present the experimental results for all prompt-based methods using ViT-L as the backbone in Table 8. REP-L outperforms competing methods in resource efficiency by bringing significant reductions in both computation time and memory usage. Importantly, REP-L is on par with its baseline model L2P in accuracy. Note that while adopting CODA-Prompt to implement REP can deliver better accuracy, its memory usage far exceeds all memory ranges under consideration.

Table 9. Extended component ablation for Split CIFAR-100. Ablating any component of REP results in lower resource efficiency by increasing training time and memory consumption.

Ablated components	Acc. ( $\uparrow$ )	Fgt. ( $\downarrow$ )	GPU Time (s)	Mem. (GB)
REP-L (ours)	86.89 $\pm$ 0.57	4.65 $\pm$ 0.14	4420.99	4.45
(1) $f_{\text{efficient}}$	86.38 $\pm$ 0.43	5.82 $\pm$ 0.81	6096.14	5.53
(2) AToM	86.43 $\pm$ 0.23	4.94 $\pm$ 0.77	7724.21	5.60
(3) ALD	86.79 $\pm$ 0.73	5.01 $\pm$ 0.39	7379.79	6.67
(4) $f_{\text{efficient}} + \text{AToM}$	85.97 $\pm$ 0.54	4.99 $\pm$ 0.73	4975.57	4.46
(5) $f_{\text{efficient}} + \text{ALD}$	86.07 $\pm$ 0.18	4.70 $\pm$ 0.66	5576.16	5.51
(6) AToM + ALD	86.08 $\pm$ 0.48	3.97 $\pm$ 0.42	5997.01	4.77

Table 10. Extended algorithm validation for Split CIFAR-100. Changing our adaptive algorithms to conventional static token merging (ToMe) or progressive layer dropping (PLD) harms model accuracy.

	Acc. ( $\uparrow$ )	Fgt. ( $\downarrow$ )	GPU Time (s)	Mem. (GB)
REP-L (ours)	86.89 $\pm$ 0.57	4.65 $\pm$ 0.14	4420.99	4.45
(1) w/ ToMe	83.55 $\pm$ 0.14	3.73 $\pm$ 0.61	5073.80	3.74
(2) w/ PLD	84.40 $\pm$ 0.35	4.88 $\pm$ 0.83	4767.86	4.46

$\circ$  ViT-L  $\square$  ViT-B  $\diamond$  ViT-Ti  $\triangledown$  RN10  $\diamond$  RN18  $\bowtie$  RN26  $+$  RN34  $\circ$  RN101  
 $\bullet$  L2P  $\bullet$  DualP  $\bullet$  CODA-P  $\bullet$  MEMO  $\bullet$  BudgetCL

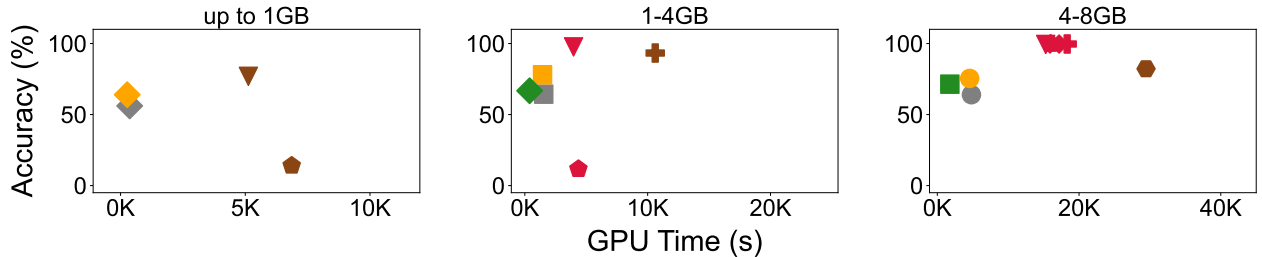


Figure 6. Extended analysis of the energy-accuracy trade-off on Split PlantDisease dataset. While CNN-based methods may excel on certain memory ranges, ViT-based methods consistently demonstrate better resource efficiency.

## E. Extended Ablation and Additional Study

As the paper mainly discusses the ablation study based on Split ImageNet-R, we here present an extended ablation study of REP using Split CIFAR-100. The results are shown in Table 9. Similar to the findings from Split ImageNet-R, the ablation of any component within REP for the Split CIFAR-100 dataset impacts resource efficiency. All components contribute to the reduction of computation time and memory usage, with AToM particularly standing out in both aspects of resource efficiency.

Furthermore, we perform algorithm validation on Split CIFAR-100, for which we present the results in Table 10. Consistent with the Split ImageNet-R results, using static token merging (ToMe) [3] or progressive layer dropping (PLD) [41] instead of adaptive token merging (AToM) or adaptive layer dropping (ALD) negatively affects model accuracy on the Split CIFAR-100 dataset. This experiment further corroborates the efficacy of our proposed algorithms in optimizing resource usage without compromising model accuracy in CL scenarios.

## F. Extended Preliminary Empirical Study

We present an extended analysis of the energy-accuracy trade-off using the Split PlantDisease dataset [26] in Figure 6. Interestingly, CNN-based methods can achieve higher accuracy on this dataset, albeit with higher computational costs. Since the PlantDisease dataset consists of localized leaf images with various disease patterns, it appears to favor CNN architectures like ResNets, which are excellent at capturing local features. On the contrary, ViT-based methods, which excel at capturing global information due to their pre-trained weights, may not perform very well on tasks requiring extensive localized feature

Table 11. Impact of REP under various computation budgets (i.e., number of iterations per task).

Method	313	625	938	1250	1563	1875
REP-L (ours)	84.06	85.47	86.60	86.66	86.57	86.89
L2P-L	84.36	86.28	87.34	87.76	87.83	88.24

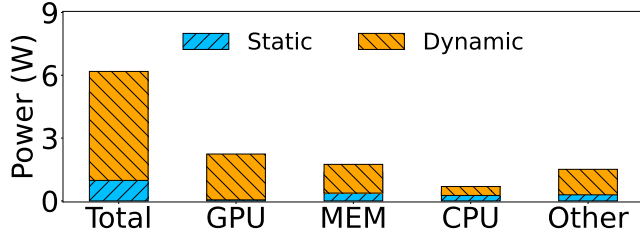


Figure 7. Power breakdown for training a ViT-B model on NVIDIA Jetson TX2.

extraction. Nonetheless, ViT-based methods demonstrate significantly greater resource efficiency. Thus, for this specific benchmark, the choice between CNN-based methods and ViT-base methods simply depends on the priority: higher resource efficiency *vs.* higher accuracy.

## G. REP under Varying Compute Budgets

We compare REP-L with L2P across various compute budgets defined by the number of iterations per task. The comparison results using Split CIFAR-100 are shown in Table 11. Evidently, the accuracy of REP-L is comparable to that of L2P across six compute budgets, with the performance gap getting increasingly marginal at lower compute budgets. We observe that the overall accuracy for both methods does not drop significantly with reduced compute budgets. This is attributed to the fact that Split CIFAR-100 is considered a less complex CL benchmark.

## H. REP on Edge Devices

Miro [23] introduces a dynamic approach for fine-tuning key design parameters of rehearsal-based CL methods to achieve high model accuracy while simultaneously reducing energy costs, i.e., high *cost-effectiveness*. Miro’s methodology centers on identifying the optimal memory size within the device’s capacity to accommodate both old and new samples for training. We compare REP with Miro directly on a reference edge device NVIDIA Jetson TX2<sup>4</sup>. This device is equipped with a 256-core NVIDIA Pascal GPU, 8GB of RAM, and a 32GB eMMC 5.1 drive. The RAM is a single unified memory shared by the CPU and GPU. We report energy usage as joules (J) obtained by multiplying power by time. Power usage is measured by reading built-in sensor values provided by Jetson devices for the GPU, RAM, CPU, and I/O connection<sup>5</sup>.

### H.1. Power Usage Breakdown

When implementing CL on edge devices, the majority of power consumption that influences energy usage during the training of a new task comes from GPU operations. Figure 7 shows power consumption on NVIDIA Jetson TX2 across individual system components. Static power is measured when the system is inactive, while dynamic power is measured during the training of a ViT-B model. During training, power usage surges up to 6.5×, with the GPU contributing 60% to the dynamic power.

### H.2. REP vs Miro

In this experiment, we explore energy-accuracy trade-offs of REP-L and Miro. Figure 8 visually represents the comparison results. In each graph, the x-axis signifies total energy usage (lower is better), while the y-axis signifies final average accuracy (higher is better). Hence, a more cost-effective strategy is positioned closer to the upper-left corner of the graph. Regarding

<sup>4</sup>NVIDIA. Jetson TX2 Module. <https://developer.nvidia.com/embedded/jetson-tx2>.

<sup>5</sup>Convenient Power Measurements on the Jetson TX2/Tegra X2 Board. <https://embeddeddl.wordpress.com/2018/04/25/convenient-power-measurements-on-the-jetson-tx2-tegra-x2-board/>.

Table 12. Comparison of REP-L with ADAM variations.

Method	Acc. ( $\uparrow$ )	GPU Time (s)	Mem. (GB)
REP-L (ours)	72.58	2542.43	4.45
VPT-Deep-L	66.70	1444.62	12.61
VPT-Shallow-L	64.53	1271.69	6.89
SSF-L	72.16	1573.70	22.09
Adapter-L	62.05	680.05	12.01

Table 13. Results on Split ImageNet-R, with ViT-L as the backbone model.

Method	Acc. ( $\uparrow$ )	Fgt. ( $\downarrow$ )	GPU Time (s)	Mem. (GB)
REP-L (ours)	75.34 $\pm$ 0.16	3.58 $\pm$ 0.29	2542.43	4.45
CODA-Prompt-L	74.43 $\pm$ 0.63	3.65 $\pm$ 0.75	6134.51	15.93
OVOR-L	75.40 $\pm$ 0.74	4.17 $\pm$ 0.65	5040.91	7.48
REP-CODA	73.30 $\pm$ 0.93	4.64 $\pm$ 0.89	5459.71	13.71
REP-OVOR	73.99 $\pm$ 0.84	4.94 $\pm$ 0.94	4486.41	7.48

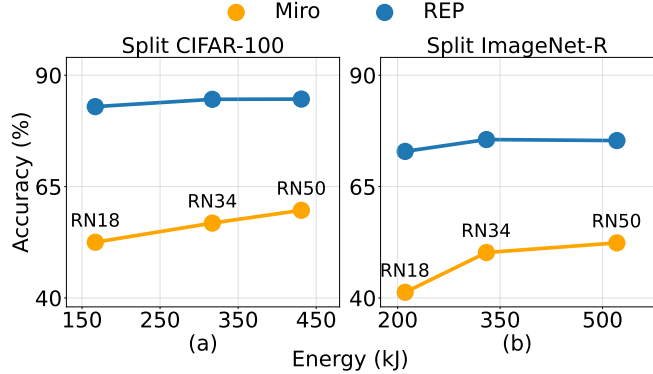


Figure 8. Energy-accuracy trade-offs for Split CIFAR100 and Split ImageNet-R between REP-L and Miro. To provide a spectrum of energy-accuracy trade-offs, we use pre-trained ResNet-18 (RN18), ResNet-34 (RN34), and ResNet-50 (RN50) for Miro.

Miro, we maintain the hyperparameters as suggested in the original work [23] but incorporate the use of pre-trained ResNet-18 (RN18; 11M), ResNet-34 (RN34; 22M), and ResNet-50 (RN50; 25M)[11] models instead of non-pre-trained ones to enhance overall performance. For REP-L, we vary the number of training iterations per task insertion to match the energy usage of Miro variants with different ResNet models.

When operating within the same energy budget, REP-L consistently outperforms Miro variants, achieving 22–33% higher accuracy across datasets. REP-L demonstrates superior cost-effectiveness, especially on Split ImageNet-R compared to Split CIFAR-100. Both REP-L and Miro prove to be memory-efficient to some extent as they fit comfortably within the on-device memory capacity. Although we explore larger ResNet models for Miro, we do not observe the accuracy levels comparable to REP-L for either dataset. This experiment also underscores the importance of specifically optimizing vision transformers for on-device CL scenarios to advance performance boundaries.

## I. Impact of Varying Hyperparameter Values

Guided by the hyperparameter tuning strategies used in DualPrompt [38] and CODA-Prompt [31], we fine-tune key hyperparameters for our ALD approach using REP-L. Our focus is primarily on optimizing the threshold parameter ( $\alpha$ ) and the adjustment factor ( $\tau$ ), which are crucial for ALD’s adaptability and efficiency. We conduct a hyperparameter search using cross-validation, for which we designate 20% of our training dataset as a validation set. Figure 9 summarizes the results. We set the AToM’s merging parameter ( $n$ ) to 8.

We also explore the impact of varying prompt-related hyperparameters, as detailed in Figure 10. Note that computational

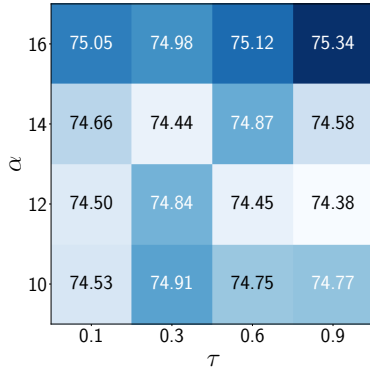


Figure 9. Result for ALD’s hyperparameter tuning via cross-validation.

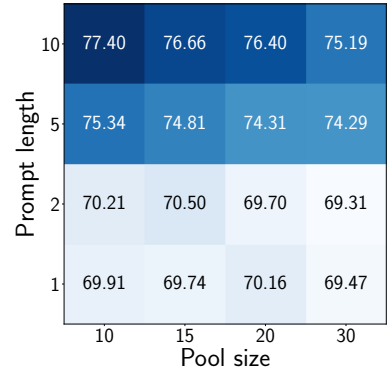


Figure 10. Impact of prompt-related hyperparameters of REP. Note that when we increase the pool size and prompt length, there is a notable increase in computation cost.

costs increase with larger prompt sizes and longer prompt lengths, and higher costs do not always translate into improved accuracy. Based on Figure 10, we opt for a prompt pool size of 10 and a prompt length of 5 to strike the right balance between computational efficiency and model accuracy.

## J. Additional Related Works

### J.1. Adapter-based Rehearsal-free Methods

Considering ADAM [44] as a state-of-the-art method for adapter-based CL, we evaluate all its variations proposed in [44] on Split ImageNet-R with 20 tasks and compare their final average accuracies with REP-L in Table 12. ADAM significantly reduces end-to-end training costs using an adapter model. Unlike REP-L, which performs the backward pass to update prompts, ADAM only updates the FC layers without the backward pass. However, training such a model is memory-intensive and often exceeds on-device memory capacity. Also, when implemented with the pre-trained ViT-L model, ADAM’s capability for generalization seems to be somewhat restricted. This observation does not necessarily indicate a fundamental limitation of ADAM but rather underscores the complexities of using it effectively in its current form.

### J.2. Advantages of REP over NAS

While NAS (Neural Architecture Search) can be integrated into REP to drop some layers, it usually involves searching the model from scratch, which is time-consuming. In contrast, our method applies adaptive schedules directly to an existing pre-trained model, significantly saving computation time. So, it can naturally adapt to device-internal resource conditions without relying on external server resources.

### J.3. Online or Few-shot CL

In on-device CL, the memory capacity for storing data from new tasks may be limited. Thus, one might consider adopting online or few-shot CL methods to save memory costs, as they require fewer new-task samples to be maintained in memory. Offline CL (our setting) typically yields better accuracy with higher resource usage. However, memory allocation for new samples is not a major constraint in offline CL. All prompt-based methods require 155–269MB to store new samples for both Split CIFAR-100 and Split ImageNet-R, accounting for only 3.4–5.9% of REP’s memory usage. Moreover, modern DL frameworks can store data in storage and proactively prefetch upcoming mini-batches for training, virtually eliminating memory concerns for new samples.

### J.4. Prompting in Self-Supervised CL

Although our REP framework is designed for conventional supervised CL, we believe it can naturally extend to self-supervised prompt-based CL methods like HiDe-Prompt [34]. By combining REP’s resource-efficient techniques with hierarchical prompt optimization, this integration could enable on-device CL for large unlabeled datasets. Such a hybrid

approach would preserve the performance benefits of prompt tuning while significantly reducing computational and memory overhead, making self-supervised CL more feasible on resource-constrained devices.

## K. REP on Diverse Prompting Methods.

In this experiment, we evaluate the performance and applicability of REP in approaches that directly update a single prompt without relying on prompt selection. CODA-Prompt [31] and OVOR [14] stand out as representative methods. We present experimental results using the Split CIFAR-100 and Split ImageNet-R datasets with a ViT-L backbone in Table 13. REP offers moderately improved resource efficiency when applied to CODA-Prompt and OVOR. During the prompt update, we were able to apply ALD without modifications, whereas AToM’s main logic required reimplementation to function with CODA-Prompt and OVOR. This does not indicate a fundamental limitation of REP’s core design but highlights the need to address this implementation challenge in future work. Nonetheless, we note that REP’s baseline accuracy and resource efficiency (the first row in Table 13) significantly outperform those observed in CODA-Prompt and OVOR.